SCIENTIFIC REPORTS
nature research

OPEN

Amorphous $Ta_xMn_yO_z$ Layer as a Diffusion Barrier for Advanced Copper Interconnects

Byeong-Seon An[1], Yena Kwon[1], Jin-Su Oh[1], Miji Lee[2], Sangwoo Pae[2] & Cheol-Woong Yang[1*]

An amorphous $Ta_xMn_yO_z$ layer with 1.0 nm thickness was studied as an alternative Cu diffusion barrier for advanced interconnect. The thermal and electrical stabilities of the 1.0-nm-thick $Ta_xMn_yO_z$ barrier were evaluated by transmission electron microscopy (TEM) and current density–electric field (*J–E*) and capacitance–voltage (*C–V*) measurements after annealing at 400 °C for 10 h. X-ray photoelectron spectroscopy revealed the chemical characteristics of the $Ta_xMn_yO_z$ layer, and a tape peeling test showed that the $Ta_xMn_yO_z$ barrier between the Cu and SiO_2 layers provided better adhesion compared to the sample without the barrier. TEM observation and line profiling measurements in energy-dispersive X-ray spectroscopy after thermal annealing revealed that Cu diffusion was prevented by the $Ta_xMn_yO_z$ barrier. Also, the *J–E* and *C–V* measurements of the fabricated metal-oxide-semiconductor sample showed that the $Ta_xMn_yO_z$ barrier significantly improved the electrical stability of the Cu interconnect. Our results indicate that the 1.0-nm-thick $Ta_xMn_yO_z$ barrier efficiently prevented Cu diffusion into the SiO_2 layer and enhanced the thermal and electrical stability of the Cu interconnect. The improved performance of the $Ta_xMn_yO_z$ barrier can be attributed to the microstructural stability achieved by forming ternary Ta-Mn-O film with controlled Ta/Mn atomic ratio. The chemical composition can affect the atomic configuration and density of the Ta-Mn-O film, which are closely related to the diffusion behavior. Therefore, the 1.0-nm-thick amorphous $Ta_xMn_yO_z$ barrier is a promising Cu diffusion barrier for advanced interconnect technology.

A copper (Cu) interconnect can transmit clock and other signals for providing power/ground functions to various microelectronic devices. Cu interconnects require a liner/barrier to improve the adhesion between the Cu and silicon-based interlayer dielectric (ILD) materials and to block the diffusion of Cu into the ILD materials[1]. A dual Ta/TaN barrier formed by physical vapor deposition (PVD) is generally used as a diffusion barrier as it leads to good adhesion between Cu and the ILD materials, in addition to ensuring thermal stability and blocking the diffusion of Cu into the ILD material[2,3]. However, the dual Ta/TaN barrier is naturally thicker than a single barrier and can increase the electrical resistivity because it occupies a larger portion of Cu line volume in the Cu interconnect. In addition, with the scaling down expected by Moore's Law[4], the conventional dual Ta/TaN diffusion barrier faces technological limitations[5], including poor step coverage by PVD methods[6] and an inability to form a barrier layer with a thickness of 1 nm or less. Recently, thinner TaN barriers prepared by atomic layer deposition (ALD) have been investigated, but their performance as barriers is not yet perfect, making them difficult to apply in practice[7].

Instead of a dual Ta/TaN barrier which has polycrystalline structure with inherent grain boundary diffusion pathways, an amorphous Ta_2O_5 barrier was investigated as a potential single barrier for Cu interconnects[8,9]. This oxide has a high thermal stability and is not reactive with Cu or SiO_2. Salaum *et al.*[8,9] reported that a 20-nm-thick amorphous Ta_2O_5 barrier showed a good performance as a diffusion barrier up to 600 °C, but it failed at higher temperatures, corresponding to the beginning of crystallization. Moreover, although amorphous Ta_2O_5 layers have some advantages as diffusion barriers, a Ta_2O_5 layer with a thickness less than 20 nm is not suitable for use as a Cu diffusion barrier because it is deposited as a discontinuous layer[8].

A notable progress in Cu interconnects is a self-forming barrier proposed by Koike *et al.*[10] The self-forming barrier was realized by spontaneously reacting the Cu–*X* alloying element with O and Si elements in the ILD material during post-metallization annealing[5]. Among the Cu–*X* alloying elements used[11–16], an Mn alloying element[17,18] is widely used because the self-formed Mn oxide or Mn silicate has good reliability and is thinner

[1]School of Advanced Materials Science and Engineering, Sungkyunkwan University, Suwon, 16419, Korea. [2]Samsung Foundry Business, Samsung Electronics, GiHeung, 17113, Korea. *email: cwyang@skku.edu

than the dual Ta/TaN barrier. The thickness of the self-forming barrier is determined by the temperature of post-metallization annealing and the type of deposition method, such as PVD, chemical vapor deposition (CVD), or ALD[19–22]. Although the CVD method yields good step coverage, Nguyen *et al.*[23] reported that it is difficult to control the barrier thickness due to the high reactivity of the Mn precursor with the SiO_2 layer, and thus amorphous $MnSi_xO_y$ diffusion barriers with thicknesses of less than 2.0 nm are not suitable for use as Cu diffusion barriers. Moreover, the self-forming barrier is very sensitive to the processing conditions such as temperature, annealing time, and alloying concentration.

On the other hand, a MnO_x layer formed by ALD was considered a good candidate because of its thickness controllability. However, it was found to act as a Cu diffusion barrier only when its thickness was greater than 1.2 nm[20]. Furthermore, the thickness of the ALD–MnO_x layer is affected by the adsorbed moisture on the substrate. The ALD–MnO_x layer was very thin on the hydrophobic surface of a low-k SiOCH substrate, whereas it was thicker on a TEOS–SiO_2 substrate[24]. Thus, the surface conditions of the ILD material are very important in terms of controlling the thickness of the ALD–MnO_x layer.

An alternative Cu diffusion barrier is required to meet various requirements such as good adhesion between Cu and the SiO_2 layer, back-end-of-line (BEOL)-compatible deposition processes, and reliability in advanced Cu interconnects[25,26]. It is desirable to avoid forming polycrystalline films with inherent grain boundaries which dominates diffusion especially at low temperatures. Therefore, the amorphous structure is still beneficial at preventing the atomic diffusion[27,28]. The incorporation of an additive element in existing transition metal oxide may offer a promising method for maintaining amorphous state by interrupting the polycrystalline phase formation. In this regard, the ternary Ta-Mn-O system is of potential interest for Cu interconnects. In addition to the ability to form an amorphous structure, the electrical resistivity of the barrier layer is another important property because it has substantial influence on the effective resistivity of the Cu interconnect. However, the resistivity of the Cu interconnect is more affected by grain boundary scattering, surface scattering, and an increasing portion of the conventional barrier in the Cu interconnect than the resistivity of the barrier layer itself[26,29]. In that sense, it is very important to minimize the thickness of the barrier layer to reduce the resistivity of the Cu interconnect. Although industry-friendly Ta-based and Mn-based barriers exhibit excellent performance in Cu interconnects, it is still challenging to fabricate a Cu diffusion barrier with a thickness less than 1.2 nm that completely prevents Cu diffusion into the ILD material.

In this study, we developed an amorphous $Ta_xMn_yO_z$ layer as an ultrathin diffusion barrier for advanced Cu interconnects that had excel`lent barrier properties, such as high thermal stability and good adhesion. A 1.0-nm-thick amorphous $Ta_xMn_yO_z$ layer was prepared by using the conventional PVD method because it allows easy and systematic investigation of the fundamental properties by changing the film thickness and chemical composition. To evaluate the thermal and electrical stability of the $Ta_xMn_yO_z$ barrier, we investigated its ability to prevent Cu diffusion into the ILD material by annealing it at 400 °C for 10 h and by applying bias thermal stress under 6 MV/cm and 150 °C for 30 min. The results of this study demonstrate that the amorphous $Ta_xMn_yO_z$ layer is a promising diffusion barrier for advanced Cu interconnects.

Results and Discussion

Figure 1a shows plan-view transmission electron microscopy (TEM) images of the as-deposited $Ta_xMn_yO_z$ barrier and selected-area electron diffraction patterns (SADPs). The $Ta_xMn_yO_z$ film was in amorphous form, as seen in the plan-view TEM image, and the SADP in the inset reveals only a halo-ring pattern, indicating a perfectly amorphous structure. The thickness of the deposited $Ta_xMn_yO_z$ barrier was determined from the cross-sectional high-resolution (HR)-TEM images of the metal-oxide-semiconductor (MOS) structure with the $Ta_xMn_yO_z$ barrier and the intensity profile (Fig. 1b,c). The intensities of the Cu, the $Ta_xMn_yO_z$ barrier, and the SiO_2 layers were different in the HR-TEM image as shown in Fig. 1c, and the $Ta_xMn_yO_z$ barrier was clearly distinguished between the Cu and SiO_2 layer. The thickness of the barrier was 1.0 nm and it was an amorphous phase. To confirm the elemental distribution in the as-deposited MOS capacitor with the $Ta_xMn_yO_z$ barrier, the scanning TEM-electron energy loss spectroscopy (STEM-EELS) spectrum was obtained in the energy loss range for each region with Cu ($L_{2,3}$ edge:931 eV), Ta (O_1 edge:71 eV), Mn (L_3 edge:640 eV), O (K edge:532 eV), and Si (K edge:99 eV). As shown in the Ta map ranging from 69.5 to 79.5 eV and the Mn map ranging from 637.5 to 647.5 eV, the $Ta_xMn_yO_z$ film was a thin layer between the Cu and SiO_2 layers (Fig. 1d).

To obtain the chemical information of the $Ta_xMn_yO_z$ diffusion barrier, X-ray photoelectron spectroscopy (XPS) analysis was performed and the results are shown in Fig. 2. The experimental XPS spectra were deconvoluted using Gaussian–Lorentzian peaks after background extraction. As shown in Fig. 2a, the Ta 4f spectrum revealed that Ta $4f_{5/2}$ and Ta $4f_{7/2}$ existed at peak values of 25.8 eV and 27.7 eV, respectively, and the loss feature for Ta_2O_5 appeared at 36.8 eV. These peaks corresponded to the binding energy of fully oxidized stoichiometric Ta_2O_5, which was in good agreement with previous work[30]. Fig. 2b shows the XPS spectrum of Mn 2p in the $Ta_xMn_yO_z$ diffusion barrier. The main two peaks with binding energies at 641.2 eV and 653.4 eV corresponded to Mn $2p_{3/2}$ and Mn $2p_{1/2}$, respectively. Peak fitting was conducted for Mn $2p_{3/2}$, which was deconvoluted into Mn^{2+}, Mn^{3+}, and Mn^{4+}, with characteristic binding energies at 640.7 eV, 641.8 eV, and 643.1 eV, respectively[31,32]. The Mn $2p_{3/2}$ peak also demonstrated an MnO satellite feature at 646.2 eV. The Mn metal in the $Ta_xMn_yO_z$ barrier consisted of MnO, MnO_2, and Mn_2O_3 based on the obtained binding energy at the Mn $2p_{3/2}$ peak. In Fig. 2c, there were three O 1 s peaks at 530.1 eV, 531.2 eV, and 532.9 eV, indicating metal–oxide (M–O), metal–oxygen vacancy ($M–O_{vac}$), and metal–hydrogen lattice (M–OH) bonds, respectively[33]. The M–O, $M–O_{vac}$, and M–OH bonds were formed by binding with the Ta and Mn metals in the $Ta_xMn_yO_z$ diffusion barrier.

Because the rough surface of the diffusion barrier can provide a fast diffusion pathway for Cu migration across the liner, the surface roughnesses of the 1.0-nm-thick $Ta_xMn_yO_z$ layer and the SiO_2 layer without the barrier (reference) were measured using atomic force microscopy (AFM). A smooth surface with a root mean square (RMS) value of 0.20 nm was obtained for the 1.0-nm-thick $Ta_xMn_yO_z$ barrier, which was similar to the RMS of the

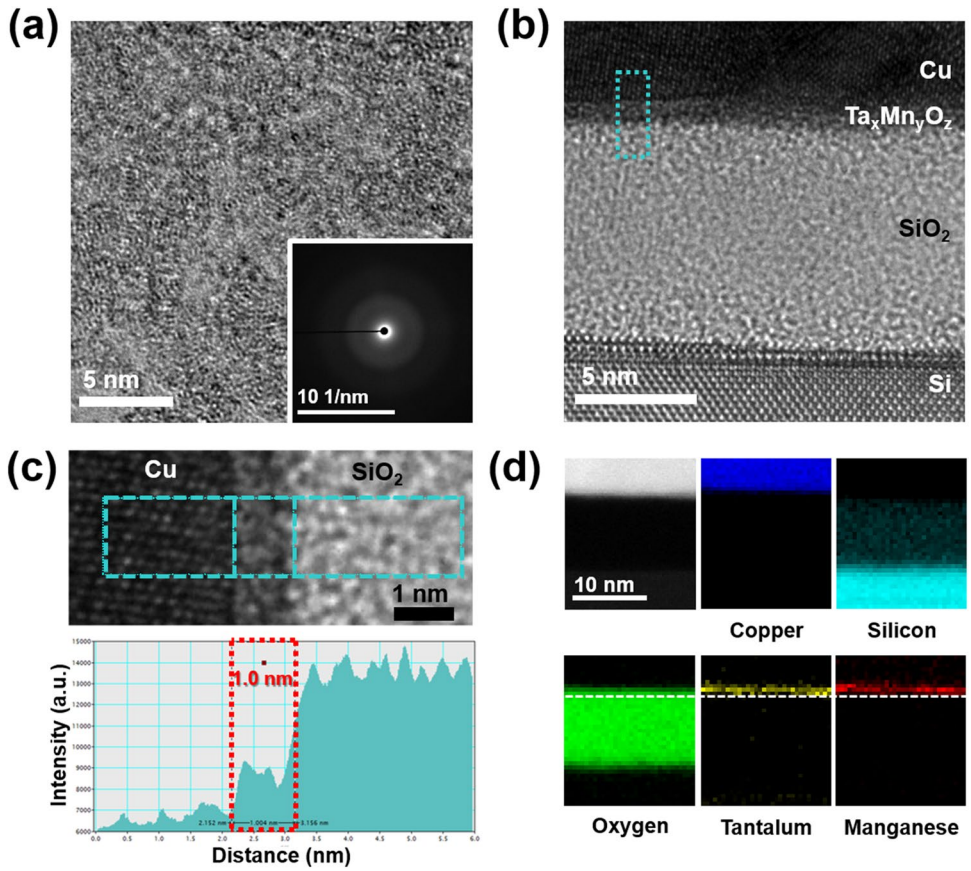

Figure 1. (**a**) Plan-view HR-TEM image showing the amorphous $Ta_xMn_yO_z$ layer. The SADP is shown in the inset. (b) Cross-sectional HR-TEM image of the as-deposited MOS capacitor sample with the amorphous $Ta_xMn_yO_z$ barrier. (**c**) Intensity profile for the thickness measurement of the initial $Ta_xMn_yO_z$ barrier. (**d**) STEM-EELS elemental maps of the as-deposited MOS capacitor sample with the amorphous $Ta_xMn_yO_z$ barrier.

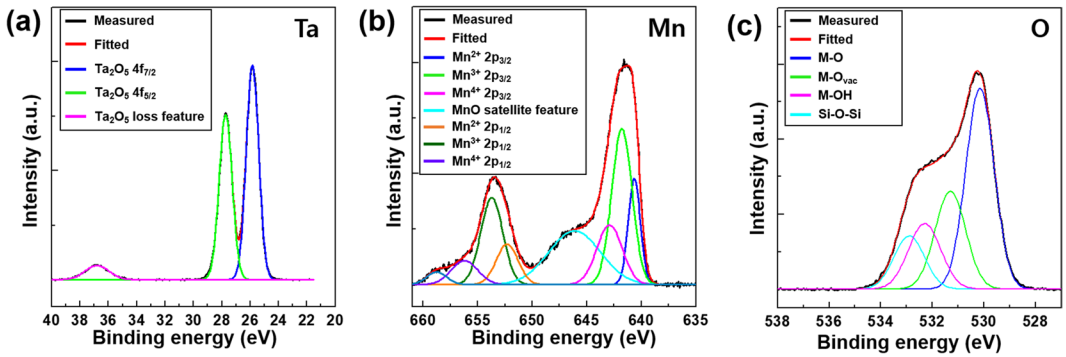

Figure 2. Representative XPS spectra of the as-deposited $Ta_xMn_yO_z$ barrier, (**a**) Ta 4f, (**b**) Mn 2p, and (**c**) O 1s.

10-nm-thick SiO_2 layer (0.19 nm), as shown in Fig. 3a,b. To examine the Cu adhesion to the SiO_2 surface resulting from the $Ta_xMn_yO_z$ barrier, 3 M Scotch tape peeling tests were performed for the MOS capacitor samples with and without the $Ta_xMn_yO_z$ barrier. As shown in Fig. 4a,b, the MOS capacitor sample without the barrier failed the tape peeling test owing to poor adhesion, which was apparent from the removal of the Cu dot electrodes. In contrast, for the $Ta_xMn_yO_z$ barrier sample, the Cu dot electrodes deposited on the SiO_2 layer did not change after the tape peeling test, as shown in Fig. 4c,d, despite multiple attempts to tear off the Cu dot electrodes. These results indicate that the $Ta_xMn_yO_z$ barrier had good adhesion between the Cu and SiO_2 layers.

To investigate the thermal stability of the 1.0-nm-thick $Ta_xMn_yO_z$ barrier, we annealed the MOS capacitor samples with and without the $Ta_xMn_yO_z$ barrier at 400 °C for 10 h. Figure 5 shows the cross-sectional HR-TEM images and the line profile of the chemical composition for each element after annealing at 400 °C for 10 h. To compare the results with and without the $Ta_xMn_yO_z$ barrier, a MOS capacitor sample without a barrier was

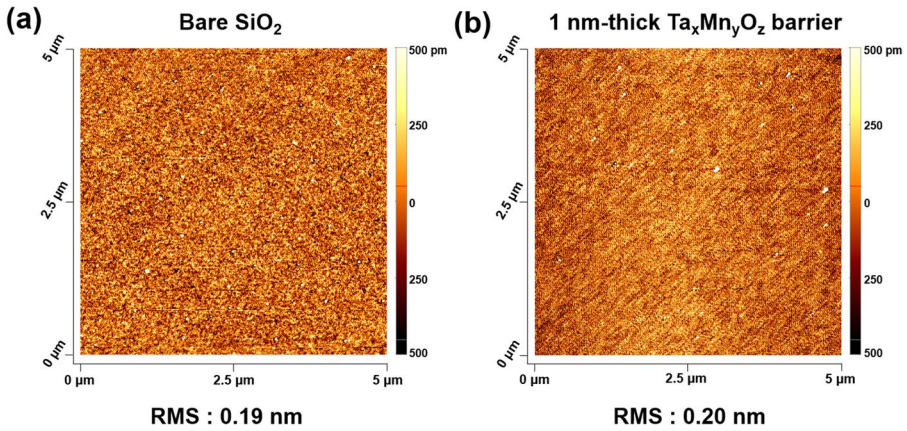

Figure 3. AFM images of the (**a**) bare SiO_2 layer as a reference and the (**b**) 1.0-nm-thick $Ta_xMn_yO_z$ barrier.

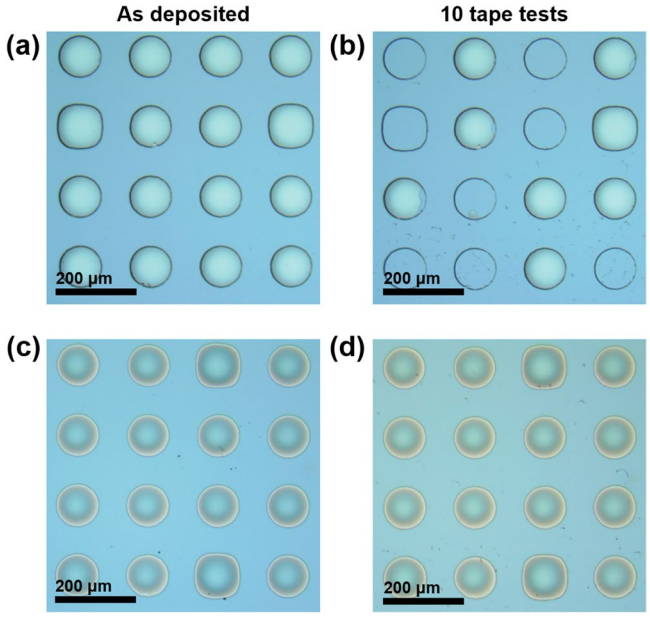

Figure 4. Optical microscope images of the as-deposited sample without the barrier (**a**) before the tape peeling test and (**b**) after 10 tape peeling tests, and the as-deposited sample with the amorphous $Ta_xMn_yO_z$ barrier (**c**) before the tape peeling test and (**d**) after 10 tape peeling tests.

prepared as a reference. For the sample without the $Ta_xMn_yO_z$ barrier, the interface between the Cu and SiO_2 layer showed a noticeable difference because of Cu diffusion into the SiO_2 layer during annealing, as shown in Fig. 5a. The initial SiO_2 layer with a thickness of 10 nm was reduced to approximately 5.8 nm owing to Cu diffusion. Conversely, the annealed sample with the $Ta_xMn_yO_z$ barrier was identical to the initial interface between the Cu and SiO_2 layers and had a uniform thickness of 1.0 nm, which was consistent with the as-deposited $Ta_xMn_yO_z$ barrier before annealing, as shown in Fig. 5b,c. In addition, the STEM-energy dispersive X-ray spectroscopy (STEM-EDS) line profile, shown in Fig. 5d,e, was used to accurately evaluate the Cu diffusion. For the sample without the $Ta_xMn_yO_z$ barrier (see Fig. 5d), Si and O were detected in the SiO_2 layers, as shown in the high-angle annular dark-field (HAADF) STEM image, and the distribution of Cu showed that the Cu atoms diffused into the SiO_2 layer. The annealed $Ta_xMn_yO_z$ diffusion barrier showed the same chemical binding states as the as-deposited $Ta_xMn_yO_z$ barrier, as shown in Fig. S1 of the SI. In the STEM-EDS line profile of the annealed sample with the $Ta_xMn_yO_z$ barrier shown in Fig. 5e, Cu was not detected inside the SiO_2 layer, which indicated no diffusion of Cu into the SiO_2 layer. However, the Ta and Mn in the diffusion barrier were not properly detected in the barrier region between the Cu and the SiO_2 layers, despite the presence of the $Ta_xMn_yO_z$ barrier. In fact, the quantitative analysis using STEM-EDS for Ta in the MOS capacitor sample was difficult because the Ta Mα (1.71 keV) and Ta Lα (8.14 keV) X-ray energies overlapped with the Si Kα (1.74 keV) and Cu Kα (8.04 keV) X-ray energies, respectively. In addition, Mn was difficult to detect in the line profile owing to the damage caused by the 200-keV e-beam during the STEM-EDS analysis. To complement STEM-EDS, Ta and Mn were confirmed using STEM-EELS. As shown in Fig. 5f, Ta and Mn were detected at the interface between the Cu and SiO_2 layers. In

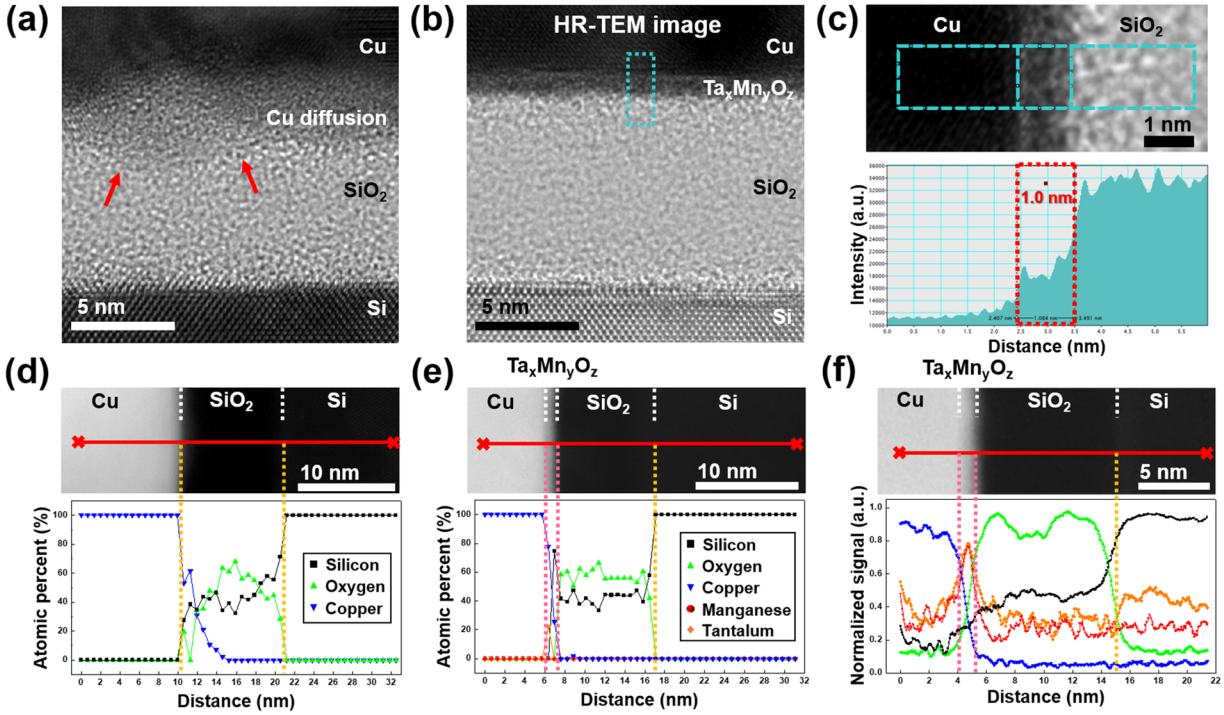

Figure 5. Cross-sectional HR-TEM images of the MOS capacitor sample (**a**) without the barrier and (**b**) with the $Ta_xMn_yO_z$ barrier. Image (**c**) shows the intensity profile for the thickness measurement after annealing at 400 °C for 10 h. The HAADF-STEM images and the STEM-EDS line profiles of the MOS capacitor sample are shown (**d**) without the barrier and (**e**) with the $Ta_xMn_yO_z$ barrier after annealing at 400 °C for 10 h. Image (**f**) shows the HAADF-STEM image and the STEM-EELS line profile of the MOS capacitor sample with $Ta_xMn_yO_z$ barrier after annealing at 400 °C for 10 h.

addition, the $Ta_xMn_yO_z$ barrier prevented the diffusion of Cu toward the SiO_2 layer, which was consistent with the Cu distribution in the STEM-EDS line profile. However, the detection of trace elements that may have affected the device characteristics was difficult because the detection limits of STEM-EDS and -EELS are approximately 0.1–3.0 wt.%[34]. Therefore, to determine the presence of a few Cu atoms in amounts as low as 10^9 atoms/cm^3 [35], the current density-electric field (*J*–*E*) and capacitance-voltage (*C*–*V*) characteristics were evaluated.

Figure 6 shows the dielectric breakdown field of a statistical time-zero dielectric breakdown (TZDB) histogram obtained using 20 *J*–*E* curves, as shown in the inset of Fig. 6 for the as-deposited and annealed MOS capacitor samples. In the statistical results of the TZDB histogram, three modes, referred to as A-, B-, and C-modes, were observed when the breakdown fields were composed of low (<1 MV/cm), intermediate, and high (>14 MV/cm) fields, respectively[36]. The A- and B-mode failures could be attributed to localized defect spots, such as Cu^+ ion transport, referred to as an extrinsic breakdown, and the C-mode failure corresponded to an approximately defect-free oxide sample, was referred to as an intrinsic breakdown. As shown in Fig. 6a,b, the MOS capacitor sample without the barrier exhibited the C-mode failure ranged from 14.25 MV/cm to 16.25 MV/cm before annealing, whereas the A- and B-mode failures ranged from 3.25 MV/cm to 12.25 MV/cm after annealing at 400 °C for 10 h. Thus, the MOS capacitor sample without the barrier exhibited extrinsic breakdown because of the Cu^+ ions that diffused into the SiO_2 layer during annealing. Conversely, in Fig. 6c,d, the $Ta_xMn_yO_z$ barrier samples exhibited C-mode failure regardless of annealing, unlike the reference sample without the barrier, and the breakdown field before and after thermal annealing ranged from 15.45 MV/cm to 16.95 MV/cm and from 15.55 MV/cm to 16.55 MV/cm, respectively. These results provide evidence that the penetration of Cu^+ ions into the SiO_2 layer did not occur, which is consistent with the TEM results shown in Fig. 5.

In addition, a correlative analysis of the XPS and *J*–*E* measurements was carried out to evaluate the performance of the 1.0-nm-thick $Ta_xMn_yO_z$ barrier layer according to the content of Ta and Mn. The Ta/Mn ratio (i.e., the normalized chemical composition of the metals) of the as-deposited $Ta_xMn_yO_z$ layer was estimated by the wide-scan XPS survey spectra, and the TZDB histogram was measured to evaluate the Cu-blocking capability of the $Ta_xMn_yO_z$ barrier after annealing at 400 °C for 10 h. Three 1.0-nm-thick $Ta_xMn_yO_z$ barriers, each with a different Ta/Mn ratio, were prepared by controlling only the deposition time during DC sputtering. As shown in Fig. S2 of the SI, the 1.0-nm-thick $Ta_xMn_yO_z$ barrier with a normalized Ta content of 91.5% (balance Mn) could not completely block Cu diffusion into the SiO_2 layer during annealing. Conversely, for the $Ta_xMn_yO_z$ barrier with normalized Ta content range from 56.5% to 62.6%, the TZDB results showed that the penetration of Cu^+ ions into the SiO_2 layer did not occur. Therefore, the chemical composition (Ta/Mn ratio) can affect the performance of $Ta_xMn_yO_z$ barrier. The incorporation of an additive element in existing binary system can lead to a change in atomic configuration and density of the barrier and contribute to maintain a high thermal stability by suppressing the polycrystalline phase formation[37–39]. Fig. S3 of the SI shows the detailed Ta 4f XPS spectrum of $Ta_xMn_yO_z$

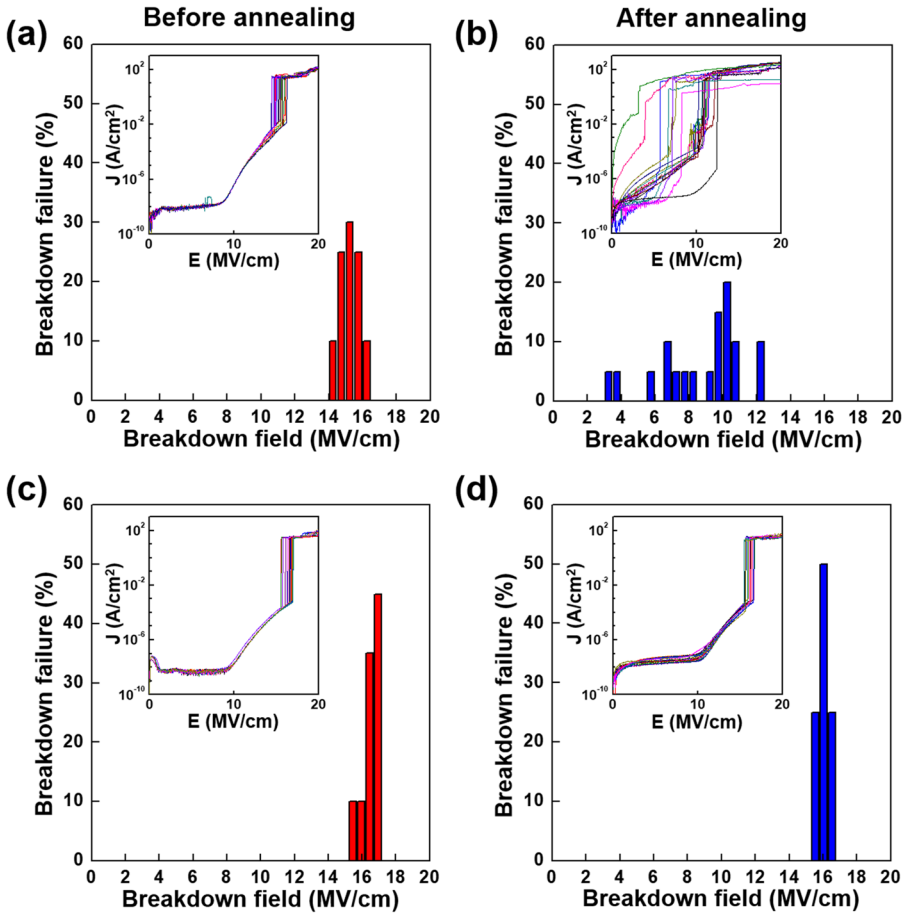

Figure 6. TZDB histogram obtained using 20 *J–E* curves for the evaluation of Cu diffusion into the SiO_2 layer following annealing at 400 °C for 10 h. The MOS capacitor sample without the barrier (*a*) before and (*b*) after annealing and with the $Ta_xMn_yO_z$ barrier (*c*) before and (*d*) after annealing.

barrier with the normalized Ta content of 91.5% in Fig. S2a. This deconvoluted Ta 4f XPS spectrum revealed that the Ta $4f_{7/2}$ and $4f_{5/2}$ binding energies corresponded to the metallic Ta as well as the amorphous Ta_2O_5, unlike $Ta_xMn_yO_z$ barrier containing the normalized Ta content of 46.55% (Fig. 2a). Therefore, the poor barrier property of the $Ta_xMn_yO_z$ layer with a high Ta/Mn ratio can be attributed to a lack of Mn and O atoms to bind Ta and the presence of metallic Ta atoms. Bassiri *et al.*[40] reported that the Ta-Ta and Ta-O bonding distances were determined as 3.1 Å and less than 2 Å, respectively, by analyzing high-quality EXAFS spectra of ion beam sputtered amorphous tantala. This implies that the amount of Ta-Ta and Ta-O bonds is closely related to the atomic configuration and density of the $Ta_xMn_yO_z$ film. Therefore, the performance of 1.0 nm-thick $Ta_xMn_yO_z$ barrier can be affected by the binding states between Ta, Mn and O, depending on the Ta/Mn ratio.

The normalized *C–V* characteristics of MOS capacitor samples with and without the $Ta_xMn_yO_z$ barrier upon annealing at 400 °C for 10 h are shown in Fig. 7. In Fig. 7a, the MOS capacitor sample without the barrier shows a negative flatband voltage shift (indicated by the green arrow) from −0.94 V to −2.54 V upon annealing owing to Cu^+ ion transport into the SiO_2 layer, which indicates a buildup of positive charge within the SiO_2 layer during annealing[18]. In addition, the hysteresis in the *C–V* curve indicates movement of the Cu^+ ion within the dielectric film during the *C–V* sweep. It was noted that the flatband voltage of the MOS capacitor with the $Ta_xMn_yO_z$ barrier before annealing was more negative than that of the as-deposited reference sample without the $Ta_xMn_yO_z$ barrier ($Cu/SiO_2/Si$). This can be attributed to intrinsic defects (positive charge was calculated as 4.63×10^{-11} C) such as charges in SiO_2 or oxygen vacancies in the $Ta_xMn_yO_z$ layer[18,41–43]. The flatband voltage moved to the positive region from −2.25 V to −0.49 V (indicated by the purple arrow) upon annealing owing to the removal of the intrinsic defects in the MOS capacitor sample and not from the diffusion of Cu^+ ions into the SiO_2 layer[18]. In other words, there was no flatband voltage shift toward the negative region, and no hysteresis curve was observed in the MOS capacitor with the $Ta_xMn_yO_z$ barrier, as shown in Fig. 7b, indicating that the Cu^+ ions were effectively prevented from diffusing into the SiO_2 layer by the $Ta_xMn_yO_z$ barrier.

The normalized *C–V* characteristics before and after bias thermal stress (BTS) were also measured. Figure 8 shows the normalized *C–V* curves for MOS capacitor with and without the $Ta_xMn_yO_z$ barrier after BTS at 6 MV/cm and 150 °C for 30 min. As shown in Fig. 8a, for the MOS capacitor without a barrier, the normalized *C–V* curve presented a roughly −1.0 V observable shift of flatband voltage toward the negative region under an electrical field of 6 MV/cm, which is consistent with the normalized *C–V* sweep after thermal annealing. Conversely,

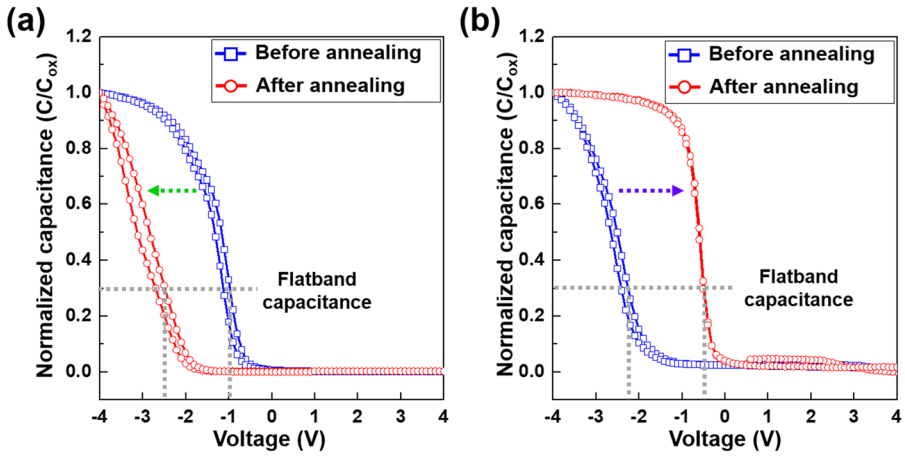

Figure 7. Normalized *C*–*V* measurements of the MOS capacitor sample (**a**) without the barrier and (**b**) with the 1.0 nm thick $Ta_xMn_yO_z$ barrier for the thermal stability evaluation.

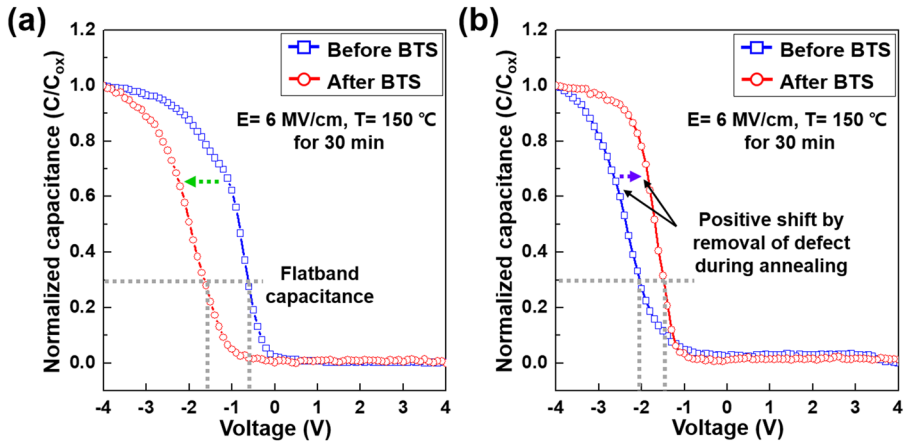

Figure 8. Normalized *C*–*V* measurements of the MOS capacitor sample (**a**) without the barrier and (**b**) with the 1.0 nm thick $Ta_xMn_yO_z$ barrier for the electrical stability evaluation under bias thermal stress.

the MOS capacitor with the $Ta_xMn_yO_z$ barrier showed no negative shift in flatband voltage, as shown in Fig. 8b. A positive shift of flatband voltage in the *C*–*V* curve occurred because of the removal of intrinsic defects during annealing.

Consequently, these results provide direct evidence that the 1.0-nm-thick amorphous $Ta_xMn_yO_z$ layer is suitable for use as an ultrathin diffusion barrier that can improve the reliability and lifetime of advanced Cu interconnects.

Conclusions

We investigated the effectiveness of an amorphous $Ta_xMn_yO_z$ layer as an ultrathin diffusion barrier for advanced Cu interconnects. A 1.0-nm-thick Ta_xMn_y layer was oxidized by exposure to air to obtain an amorphous $Ta_xMn_yO_z$ film. Ta and Mn were present as Ta_2O_5, MnO, MnO_2, and Mn_2O_3 in the amorphous $Ta_xMn_yO_z$ film. The tape peeling test for the MOS capacitor sample showed no delamination in the presence of the $Ta_xMn_yO_z$ layer, which improved the adhesion between the Cu and the SiO_2 layers. To evaluate the diffusion barrier properties of the 1.0-nm-thick amorphous $Ta_xMn_yO_z$ film, MOS capacitor samples with and without the barrier were annealed at 400 °C for 10 h. HR-TEM and STEM-EDS/EELS analyses showed that the amorphous $Ta_xMn_yO_z$ barrier had a stable microstructure and chemical composition, even after thermal annealing. The *J*–*E*, *C*–*V* and TZDB results showed that the diffusion of Cu was effectively blocked by the amorphous $Ta_xMn_yO_z$ barrier. The correlative analysis of XPS and TZDB revealed that, with a comparable O concentration, the Ta/Mn atomic ratio affected the atomic configuration and density of Ta–Mn–O films. To prevent the Cu diffusion into the Ta–Mn–O film, the Ta/Mn ratio needs to be high to ensure a high atomic density. However, the Ta/Mn ratio cannot be too high because a lack of Mn and O atoms to bind Ta and the presence of the metallic Ta atoms deteriorates the barrier performance. In conclusion, a 1.0-nm-thick amorphous $Ta_xMn_yO_z$ layer serves as an adhesion promotor and excellent diffusion barrier, and it can be used as a single liner/barrier material for advanced Cu interconnects.

Methods

The substrates for barrier deposition were 10-nm-thick SiO_2 films on p-type doped silicon (100) wafers and were cleaned using a piranha solution of 3:1 sulfuric acid (H_2SO_4) and hydrogen peroxide (H_2O_2). Then, the Mn layer was deposited first, followed by Ta layer deposition on the SiO_2/Si substrate by direct current (DC) magnetron sputtering using a Mn target (purity 99.9%) and Ta target (purity 99.99%) under a power of 5W at an Ar gas pressure of 5.5 mTorr (see Fig. S4 of the SI for the deposition process and the formation of the $Ta_xMn_yO_z$ layer). The DC sputtering chamber was pumped down to a base pressure less than 4.0×10^{-7} Torr and pre-sputtering was conducted at 10 W higher than the processing power for 20 min before deposition. The sequentially deposited ultrathin Mn and Ta films were intermixed to form a Ta_xMn_y film. The 1.0-nm-thick Ta_xMn_y film was oxidized by atmospheric exposure for the *ex-situ* sputtering to deposit the Cu film. Fig. S4 of the SI shows a schematic of the oxidation mechanism of the Ta_xMn_y film. The oxidized Ta_xMn_y film is referred to as the $Ta_xMn_yO_z$ layer. It was found that this intermixing and oxidation mechanism was valid only for sequentially deposited ultrathin Mn and Ta films with a total thickness less than 2.5 nm (see Fig S5 of the SI).

To fabricate the MOS capacitor structure, 150-nm-thick Cu films were then deposited on the $Ta_xMn_yO_z$ film by DC magnetron sputtering with dots of 100 µm diameter through a shadow mask, and a 50-nm-thick Ta film was coated as the capping layer. MOS capacitor samples with and without the 1.0-nm-thick $Ta_xMn_yO_z$ layer were prepared using the same deposition method. To evaluate the thermal stability of the $Ta_xMn_yO_z$ layer as a diffusion barrier, the as-deposited MOS capacitor samples were annealed at 400 °C for 10 h in a tube furnace under Ar + 10% H_2 gas flow. XPS (ESCALAB250Xi, Thermo-Scientific, UK) was used to determine the chemical characteristics of the deposited $Ta_xMn_yO_z$ layer. Samples for cross-sectional transmission electron microscopy (TEM) were fabricated using a focused ion beam (FIB, NX2000, Hitachi). The TEM samples were milled using a high-energy Ga^+ ion beam from 30 keV to 5 keV and a low-energy Ar^+ ion beam of 1 keV after the electron beam-induced deposition of the W material as a protective layer to minimize damage to the surface layers during the FIB milling process[44,45]. TEM (JEOL ARM-200F) analysis at 200 kV with EDS and EELS were used to analyze the microstructure and to obtain the line profiles for the chemical composition of the Cu, Ta, Mn, Si, and O elements in the two types of samples before and after annealing. The surface morphology of the 1.0-nm-thick $Ta_xMn_yO_z$ layer was analyzed by AFM (Park System Co.), and the adhesion strength between the Cu and SiO_2 layers depending on the presence of the $Ta_xMn_yO_z$ barrier was examined using a 3M Scotch tape peeling test[46].

To evaluate the Cu diffusion barrier performance of $Ta_xMn_yO_z$ after annealing at 400 °C for 10 h, the *J–E* characteristics were evaluated using a microprobe system connected to an Agilent B1500A parametric analyzer. The *J–E* curves were measured by applying voltage ranging from 0 V to −20 V in −50-mV steps. The BTS tests were performed by using a microprobe system capable of annealing and applying a high electric field to the MOS capacitor in a controlled environment. For the BTS tests, a bias field of 6 MV/cm was applied on the MOS capacitor at 150 °C for 30 min. After a given time period, the samples were cooled to room temperature. The *C–V* characteristics before and after thermal annealing and BTS were evaluated using a probe station with an Agilent E4980A precision LCR meter with an AC frequency of 100 kHz. For all *C–V* measurements, a voltage ranging from +4 V to −4 V was applied in 0.1-V steps, and the hysteresis was scanned by applying a reverse voltage of −4 V to +4 V.

Received: 11 September 2019; Accepted: 17 December 2019;
Published online: 27 December 2019

References

1. Baklanov, M., Ho, P. S., & Zschech, E. Advanced Interconnects for ULSI Technology. (John Wiley & Sons: Hoboken, 2012).
2. Hubner, R. *et al.* Structure and thermal stability of graded Ta-TaN diffusion barriers between Cu and SiO_2. *Thin Solid Films* **437**, 248–256 (2003).
3. Xie, Q. *et al.* Superior thermal stability of Ta/TaN bi-layer structure for copper metallization. *Appl. Surf. Sci.* **253**, 1666–1672 (2006).
4. Schaller, R. R. Moore's law: Past, present, and future. *IEEE Spectrum* **34**, 53–59 (1997).
5. Koike, J., Haneda, M., Iijima, J. & Wada, M. Cu Alloy metallization for self-forming barrier process. 2006 International Interconnect Technology Conference, Burlingame, CA, USA, New York: IEEE (2006, June 5–7).
6. Tsai, M. H., Sun, S. C., Tsai, C. E., Chuang, S. H. & Chiu, H. T. Comparison of the diffusion barrier properties of chemical-vapor-deposited TaN and sputtered TaN between Cu and Si. *J. Appl. Phys.* **79**, 6932–6938 (1996).
7. Wu, Z. *et al.* PVD-treated ALD TaN for Cu interconnect extension to 5 nm node and beyond. 2018 IEEE International Interconnect Technology Conference - IITC, Santa Clara, CA, USA, New York: IEEE (2018, June 4–7).
8. Salaun, A. L., Mantoux, A., Blanquet, E., Djurado, E. & ESD, A. L. D. depositions of Ta2O5 thin films investigated as barriers to copper diffusion for advanced metallization. *J. Electrochem. Soc.* **156**(5), H311–315 (2009).
9. Salaun, A. L., Mantoux, A., Djurado, E. & Blanquet, E. Atomic layer deposition of tantalum oxide thin films for their use as diffusion barriers in microelectronic devices. *Microelectron. Eng.* **87**, 373–378 (2010).
10. Koike, J. & Wada, M. Self-forming diffusion barrier layer in Cu–Mn alloy metallization. *Appl. Phys. Lett.* **87**, 041911, https://doi.org/10.1063/1.1993759 (2005).
11. Cao, F., Wu, G. H., Jiang, L. T. & Chen, G. Q. Application of Cu-C and Cu-V alloys in barrier-less copper metallization. *Vacuum* **122**, 122–126, https://doi.org/10.1016/j.vacuum.2015.09.011 (2015).
12. Hu, C. K. *et al.* Electromigration in Cu(Al) and Cu(Mn) damascene lines. *J. Appl. Phys.* **111**, https://doi.org/10.1063/1.4711070 (2012).
13. Tsukimoto, S., Morita, T., Moriyama, M., Ito, K. & Murakami, M. Formation of Ti diffusion barrier layers in thin Cu(Ti) alloy films. *J. Electron. Mater.* **34**, 592–599, https://doi.org/10.1007/s11664-005-0070-0 (2005).
14. Frederick, M. J. & Ramanath, G. Kinetics of interfacial reaction in Cu-Mg alloy films on SiO_2. *J. Appl. Phys.* **95**, 363–366, https://doi.org/10.1063/1.1630355 (2004).
15. Wang, Y., Tang, B. H. & Li, F. Y. The properties of self-formed diffusion barrier layer in Cu(Cr) alloy. *Vacuum* **126**, 51–54, https://doi.org/10.1016/j.vacuum.2016.01.019 (2016).
16. Park, J. H. *et al.* Self-forming VOx layer as Cu diffusion barrier for low-k dielectrics. *Surf. Coat. Tech.* **259**, 252–256, https://doi.org/10.1016/j.surfcoat.2014.04.003 (2014).
17. Neishi, K. *et al.* Formation of a manganese oxide barrier layer with thermal chemical vapor deposition for advanced large-scale integrated interconnect structure. *Appl. Phys. Lett.* **93**, https://doi.org/10.1063/1.2963984 (2008).

18. Byrne, C. *et al*. *In situ* XPS chemical analysis of $MnSiO_3$ copper diffusion barrier layer formation and simultaneous fabrication of metal oxide semiconductor electrical test MOS structures. *ACS Appl. Mater. Interfaces* **8**, 2470–2477, https://doi.org/10.1021/acsami.5b08044 (2016).
19. Dixit, V. K., Neishi, K., Akao, N. & Koike, J. Structural and electronic properties of a Mn oxide diffusion barrier layer formed by chemical vapor deposition. *IEEE Trans. Device Mater. Reliab*. **11**, 295–302, doi:10.1109/TDMR.2011.2141671 (2011).
20. Matsumoto, K., Maekawa, K., Nagai, H., & Koike, J. Deposition behavior and substrate dependency of ALD MnOx diffusion barrier layer. 2013 IEEE International Interconnect Technology Conference – IITC, Kyoto, Japan, New York: IEEE (2013, June 13–15).
21. Park, J. H. *et al*. Self-forming Mn-based diffusion barriers on low-k substrates. *Jpn. J. Appl. Phys*. **53**, https://doi.org/10.7567/Jjap.53.08nl01 (2014).
22. Haneda, M., Iijima, J., & Koike, J. Growth behavior of self-formed barrier at Cu-Mn/SiO2 interface at 250-450 degrees C. *Appl. Phys. Lett*. **90**, https://doi.org/10.1063/1.2750402 (2007).
23. Nguyen, M. P., Sutou, Y. & Koike, J. Diffusion barrier property of MnSixOy layer formed by chemical vapor deposition for Cu advanced interconnect application. *Thin Solid Films* **580**, 56–60, https://doi.org/10.1016/j.tsf.2015.03.007 (2015).
24. Koike, J., Hosseini, M., Hai, H. T., Ando, D., & Sutou, Y. Material innovation for MOL, BEOL, and 3D intergration. 2017 IEEE International Electron Devices Meeting (IEDM), San Francisco, CA, USA, New York: IEEE (2017, December 2–6).
25. Lo, C.-L. *et al*. Large-area, single-layer molybdenum disulfide synthesized at BEOL compatible temperature as Cu diffusion barrier. *IEEE Electron Device Lett.* **39**, 873–876, https://doi.org/10.1109/led.2018.2827061 (2018).
26. Lo, C.-L. *et al*. Enhancing interconnect reliability and performance by converting tantalum to 2D layered tantalum sulfide at low temperature. *Adv. Mater.* **31**, 1902397, https://doi.org/10.1002/adma.201902397 (2019).
27. Cao, Z. H., Hu, K. & Meng, X. K. Diffusion barrier properties of amorphous and nanocrystalline Ta films for Cu interconnects. *J. Appl. Phys.* **106**, 113513 (2009).
28. Kaloyeros, A. E. & Eisenbraun, E. Ultrathin diffusion barriers/liners for gigascale copper metallization. *Annu. Rev. Mater. Sci.* **30**, 363–385 (2000).
29. Cheng, Y. L., Lee, C. Y. & Huang, Y. L. Copper Metal for Semiconductor Interconnects. *In Noble and Precious Metals – Properties, Nanoscale Effects and Applications* (IntechOpen, 2018).
30. Abbas, Y. *et al*. Compliance-free, digital SET and analog RESET synaptic characteristics of sub-tantalum oxide-based neuromorphic device. *Sci Rep* **8**, 1228, https://doi.org/10.1038/s41598-018-19575-9 (2018).
31. Du, Y. *et al*. Mesostructured amorphous manganese oxides: facile synthesis and highly durable elimination of low-concentration NO at room temperature in air. *Chem. Commun.* **51**, 5887–5889, https://doi.org/10.1039/c5cc00269a (2015).
32. Ramirez, A. *et al*. Evaluation of MnOx, Mn2O3, and Mn3O4 electrodeposited film for the oxygen evolution reaction of water. *J. Phys. Chem. C* **118**, 14073–14081 (2014).
33. Kim, W. G. *et al*. High-pressure gas activation for amorphous indium-gallium-zinc-oxide thin-film transistors at 100 degrees C. *Sci Rep* **6**, 23039, https://doi.org/10.1038/srep23039 (2016).
34. Bart, J. C. J. Plastics Additives: Advanced Industrial Analysis. (IOS Press, 2006).
35. Pierret, R. F. Semiconductor Device Fundamentals. (Addison-Wesley Press, 1996).
36. Hori, T. *Gate Dielectrics and MOS ULSIs* (Springer, 1997).
37. Lai, L. W. & Chen, J. S. Influence of Ta/Si atomic ratio on the interdiffusion between Ta-Si-N and Cu at elevated temperature. *J. Appl. Phys.* **94**, 5396 (2003).
38. Yan, H. *et al*. Formation and characterization of magnetron sputtered Ta-Si-N-O thin films. *Thin Solid Films* **517**, 5207–5211 (2009).
39. Consiglio, S. *et al*. Atomic Layer Deposition of Ultrathin TaN and Ternary Ta1-xAlxNy Films for Cu Diffusion Barrier Applications in Advanced Interconnects. *ECS Transactions* **69**(7), 181–189 (2015).
40. Bassiri, R. *et al*. Order within disorder: The atomic structure of ion-beam sputtered amorphous tantala (a-Ta2O5). APL. *Materials* **3**, 036103 (2015).
41. McIntyre, P. C. Bulk and interfacial oxygen defects in HfO_2 gate dielectric stacks: a critical assessment. *ECS Transactions* **11**(4), 235–249 (2007).
42. Bentarzi, H. *Transport in metal-oxide-semiconductor structures: mobile ions effects on the oxide properties*. (Springer-Verlag, 2011).
43. Hosseini, M., Ando, D., Sutou, Y. & Koike, J. Co and CoTix for contact plug and barrier layer in integrated circuits. *Microelectron. Eng.* **189**, 78–84 (2018).
44. An, B. S., Shin, Y. J., Ju, J. S. & Yang, C. W. Transmission electron microscopy specimen preparation for two-dimensional material using electron beam-induced deposition of a protective layer in the focused ion beam method. *Applied Microscopy* **48**, 122–125, https://doi.org/10.9729/AM.2018.48.4.122 (2018).
45. Kato, N. I. Reducing focused ion beam damage to transmission electron microscopy samples. *J. Electron. Microsc.* **53**, 451–458, https://doi.org/10.1093/jmicro/dfh080 (2004).
46. Strong, J. On the cleaning of surfaces. *Rev. Sci. Instrum.* **6**, 97–98, https://doi.org/10.1063/1.1751951 (1935).

Acknowledgements

This study was supported by the Ministry of Trade, Industry & Energy (MOTIE) [Project Number 10080625], the Korea Semiconductor Research Consortium (KSRC) support program for the development of future semiconductor devices funded by the Korean government (MSIP). This work was also supported in part by the Korea Basic Science Institute (KBSI) National Research Facilities & Equipment Center (NFEC) grant funded by the Korea government (MOE) (No. 2019R1A6C1010031), and Samsung Electronics. The authors are grateful for support from the Cooperative Center for Research Facilities (CCRF) at Sungkyunkwan University.

Author contributions

B.S.A. contributed to the device fabrication, characterization, and data analysis and to writing the manuscript. Y.K. and J.S.O. contributed to the TEM analysis and the data analysis. M.L. and S.P. discussed the results and commented on the manuscript. C.W.Y. supervised the project, along with advising and reviewing the manuscript. All authors read and approved the final manuscript.

Competing interests

The authors declare no competing interests.

Additional information

Supplementary information is available for this paper at https://doi.org/10.1038/s41598-019-56796-y.

Correspondence and requests for materials should be addressed to C.-W.Y.

Reprints and permissions information is available at www.nature.com/reprints.